Stress Corrosion Cracking Failure of a Geothermal Steam Piping Rupture Disc

Sigit Prabowo[1], Keith Lichti[1], and Liam Norton[2]

[1]Quest Integrity NZL Limited, Block D 20 Somme Road, Upper Hutt 5018, New Zealand

[2] Mercury NZ Limited, 362B Onepu Springs Road, Kawerau, New Zealand

s.prabowo@questintegrity.com

Keywords: *Stress corrosion cracking, rupture disc, geothermal, steam piping*

ABSTRACT

Rupture discs are typically installed on the high-pressure carbon steel geothermal steam piping as a safety overpressure protection device. In a geothermal power station, a rupture disc burst without any evidence of an overpressure event. The rupture disc was rated for 17 bar, well above the steam piping operating pressure of 12 bar. This paper presents failure analysis results of the burst event of this rupture disc. The results indicated that the primary damage mechanism was chloride stress corrosion cracking (Cl-SCC), which led to change in the stress distribution on score lines and compromised the disc integrity. This paper also discusses materials selection options for the rupture disc with better resistance to Cl-SCC.

1. INTRODUCTION

In a geothermal power station, a rupture disc on the high-pressure carbon steel geothermal steam piping experienced burst without any recorded over-pressure event during operation. The rupture disc was rated for 17 bar, while the operating pressure of the steam piping was 12 bar of geothermal steam. The age of the rupture disc was approximately 12 years. There was no definite design life for the rupture disc, and it was made of 316 stainless steel UNS S31600.

Several rupture discs were installed along the high-pressure steam piping, but only one failed. Each rupture disc was enclosed in a pipe facing upward. The outside of the burst disc was facing upward at atmospheric pressure. There was a rain cover at the top of each upward pipe. However, the rain cover did not tightly enclose the pipe. The outer atmospheric conditions might have included rainwater and hydrogen sulphide from nearby vents.

The failed rupture disc was a forward-acting type that acted as a sacrificial pressure relief device. The rupture disc had two defined score marks on the dome where the rupture was designed to begin, as shown in Figure 1 (a). The concave side of the dome faced the high-pressure steam, while the convex side faced the atmosphere. In an over-pressure event, the rupture disc was designed to open along the two score lines in a petal fashion.

The failure mode of the current failed rupture disc was considered unusual. The disc opened on one of the score lines, but it was deformed upward along the score line instead of the petal burst, as shown in Figure 1. This failure mode was unlikely to have been caused by an over pressure event. This paper presents the investigation results of the unusual failure mode of the rupture disc.

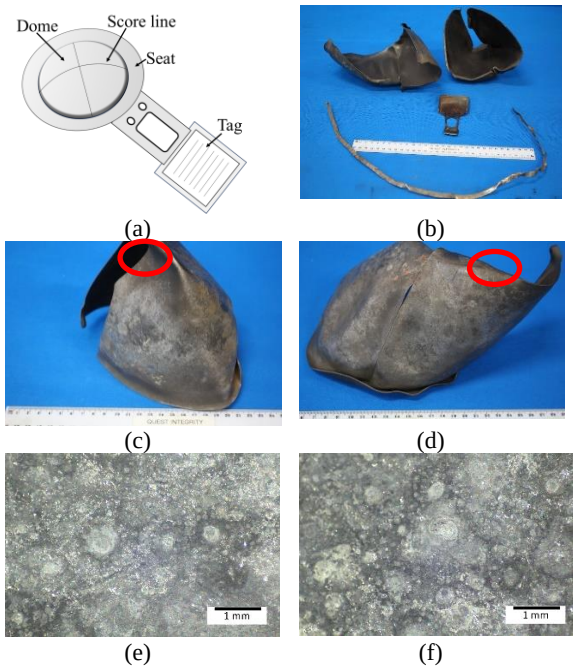

Figure 1: Schematic figure of the rupture discs and photographs of the as-received failed rupture disc (b). (c) shows Disc piece 1 and (d) shows Disc piece 2. (e) and (f) show numerous pitting on the convex side of the rupture disc. The red circles indicate the location of the cracking.

2. ANALYSIS RESULTS

2.1 Visual Examination

As-Received Condition

The as-received failed rupture disc samples were examined visually, and Figure 1 shows the photographs of the disc sample. The seat and the tag were dislodged from the original assembly. The measured score depth was approximately 0.2 mm within the disc full thickness of approximately 1.2 mm. The disc split into two pieces along one of the original score lines. For convenience, the two-piece of the disc was arbitrarily named Disc Piece 1 (Figure 1 (c)) and Disc Piece 2 (Figure 1 (d)).

Numerous fine pits were observed on the convex side, see Figure 1 (e) and (f). A small section of the disc sample (60 × 50 mm) was cut and chemically cleaned for pitting survey. These fine pits had an average pit depth of less than 15 μm as measured by an optical microscope.

Cracking

Cracking was observed only on the convex side exposed to the atmosphere. The cracking was approximately 60 mm from

the centre of the crossed score line, as highlighted by the red circle in Figure 1 (c). Cracking was also observed on the matching face on the other disc piece, as shown in Figure 1 (d).

Cracks were further examined using a binocular microscope. Figure 2 and Figure 3 show photographs of cracks observed at the red circle mark areas shown in Figure 1. The following were observed:

- A crack was observed to have propagated from a notch near the score line, as shown in Figure 2 (a). This crack was connected to another crack that propagated from a pit. In addition, two cracks were also observed at approximately 1 mm away from the notch area (Figure 2 (b)).
- The cracking was observed to be branching from the score line (Figure 2 [c] and Figure 3 [a]).
- Longitudinal cracking was also present along the cross-section of the score line, see Figure 2 (c) and Figure 3 (b).

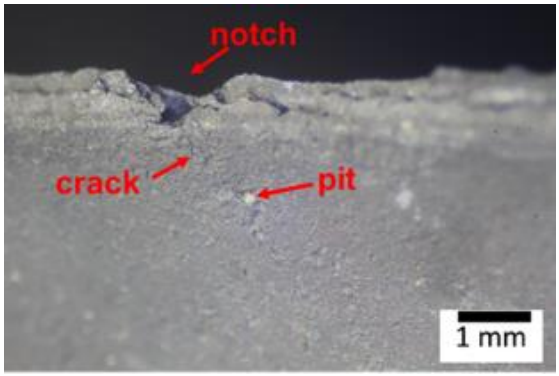

(a) A crack propagated from a notch and a pit near the edge of the score line.

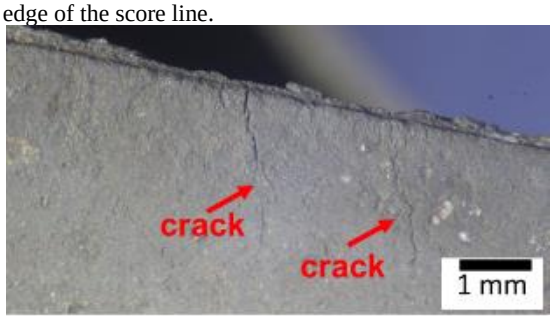

(b) Cracks propagated from the edge of the score line.

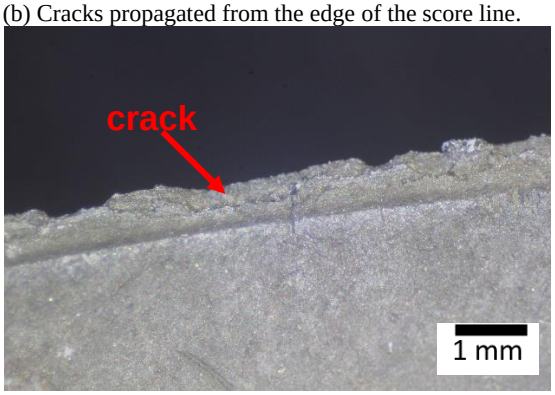

(d) A longitudinal crack along the score line.

Figure 2: Photograph of cracks observed at the edge of the score line of the disc piece 1 at the area marked by a red circle in Figure 1 (c).

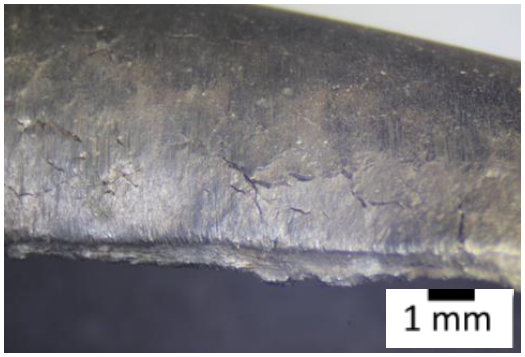

(a) Cracks branching from the score line.

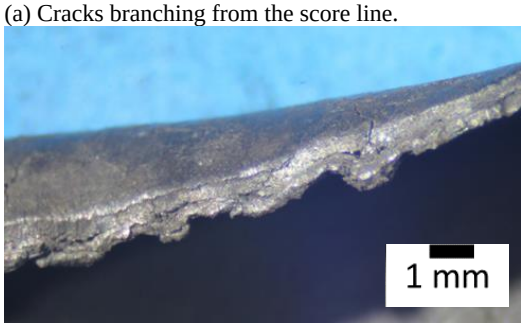

(b) A longitudinal crack along the cross-section of the score line.

Figure 3: Photograph of cracks observed at the edge of the score line of the disc piece 2 at the area marked by red circle in Figure 1 (d).

2.2 Microscopic Analysis

2.2.1 Electron Microscopy

Electron microscopy analysis in this work used a scanning electron microscope (SEM) equipped with an electron dispersive spectroscopy (EDS) detector. The EDS was used to analyze the elemental composition of the areas of interest. For the analysis, a section was cut at the location near the cracking described in Section 2.1 from Disc piece 1 for analysis of any deposit present on the surface. The sample was carefully cut using a hacksaw without any cleaning liquid to prevent contamination from the sample preparation. A matching section from Disc piece 2 was also cut and cleaned for the observation of the cracking structure.

Disc Piece 1, Deposit Contamination

Figure 4 shows low magnification secondary electron (SE) SEM images of the crack at the notch shown in Figure 2 (a). High magnification SEM images are shown in Figure 5, together with the EDS analysis on the highlighted areas (Table 1). The EDS analysis indicated chloride contaminant near the notch and the cracking. In Figure 5 (a), possible NaCl was observed on points 1 and 2. Note, chloride is easily dissolved in water. The residual low concentration of chloride (0.5-2.3 wt.%) detected by EDS was enough to indicate the presence of significant chloride contamination. Apart from chloride, a high amount of corrosive species such as sulphur (7-15 wt.%) and contaminants such as magnesium, calcium, silicon, aluminum, and potassium were detected.

Disc Piece 2, Crack Structure

Figure 6 shows the SE-SEM image of cracks on the disc piece 2 sample. The figure shows multiple cracks with branching on both the convex side (a) and on the score line (b).

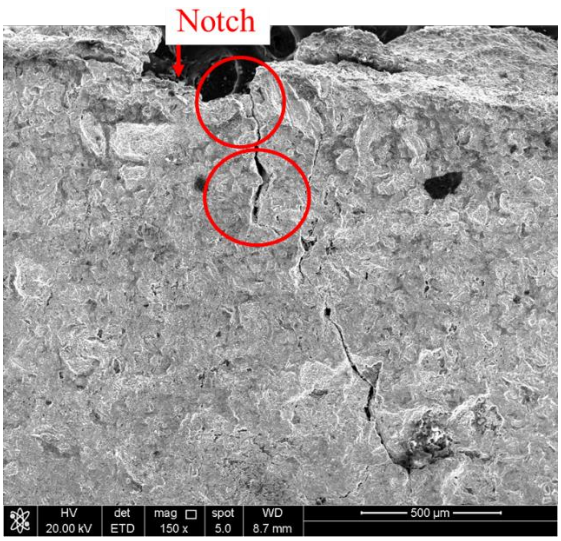

Figure 4: Low magnification SE-SEM images of the crack at the notch shown in Figure 2 (a).

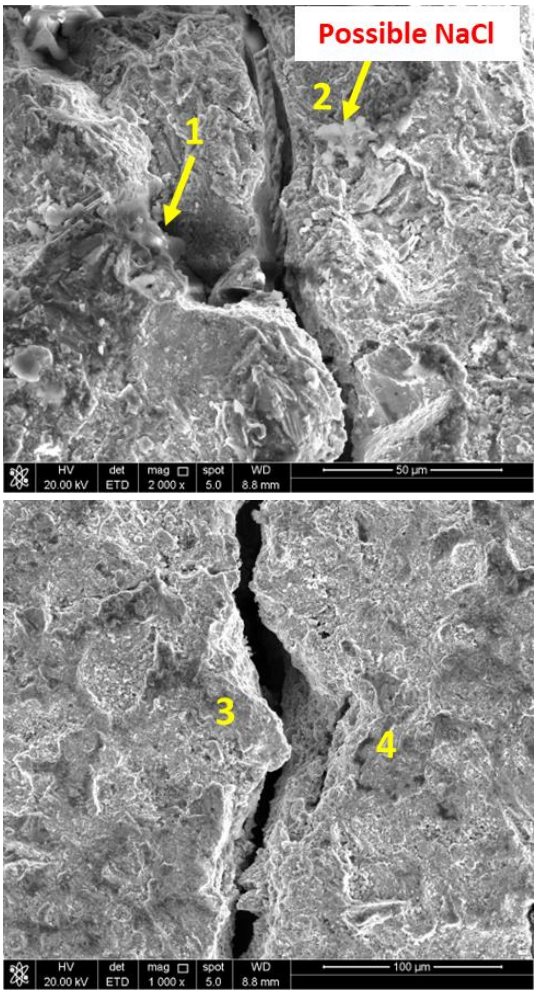

Figure 5: High magnification SE-SEM images of red circle marked areas in Figure 4.

Table 1: EDS point analysis inside the numbered spots in Figure 5.

Element	Spot (Wt.%)			
	1	2	3	4
O	25.05	13.76	12.5	8.3
Na	7.81	4.78	1.4	2.2
Mg	2.19	0.8	-	-
Al	1.56	1.85	-	-
Si	1.17	3.38	0.2	0.6
S	9.64	7.15	15.8	7.6
Cl	1.95	2.3	0.5	0.5
K	2.51	0.76	0.6	0.5
Ca	0.68	2.43	-	-
Cr	7.57	9.57	8.9	13.9
Mn	0.65	1.29	0.9	1.4
Fe	35.79	48.18	55.4	58.4
Ni	3.42	3.45	3.8	6.6
Co	-	0.29	-	-

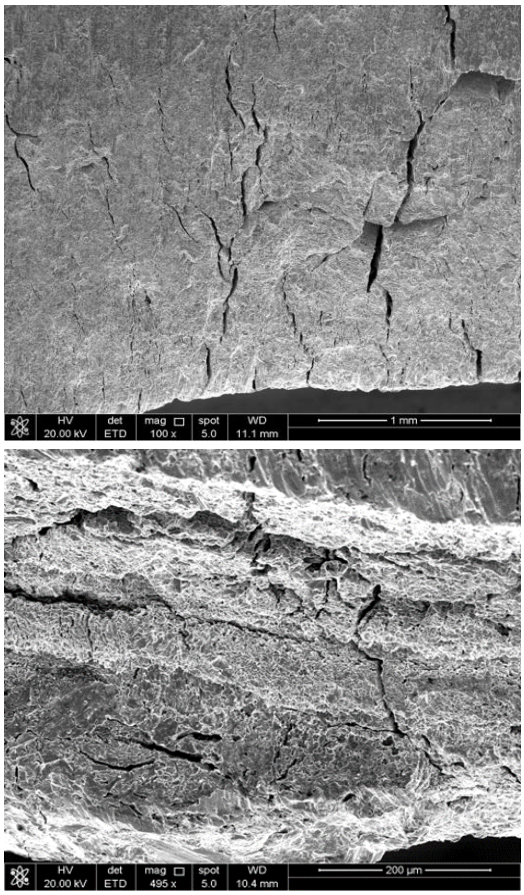

Figure 6: SE-SEM images showing crack branching near the edge at the location shown in Figure 3, Disc piece 2. (a) is top view of the convex side. (b) is the cross-section of the cracking along the score line.

2.2.2 Metallurgical Examination

As described in Section 2.1, multiple cracks with branching were observed. A micro-specimen was prepared from section of Disc piece 2 sample shown in Figure 3. The micro-specimen was then ground and polished to a 1-µm finish.

Figure 7 shows the polished cross-section of the sample. Cracks appeared to be branching from the corroded surface and from the likely high-stress area near the crossed-score line, see Figure 7 (a). Several pits were also observed near the cracks at the external surface, as indicated by red arrows in Figure 7 (a). In contrast, there was no cracking in the non-corroded area, as shown in Figure 7 (b).

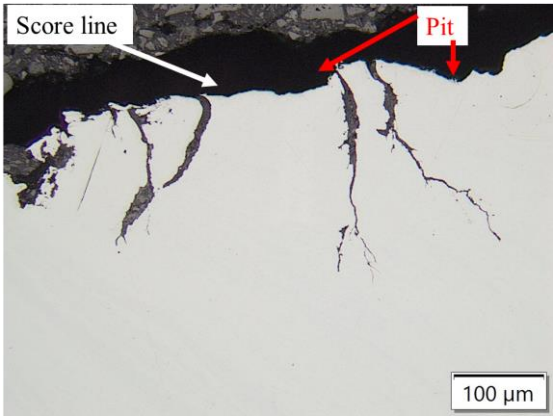

(a) Cracks branching from the corroded surface of the score line.

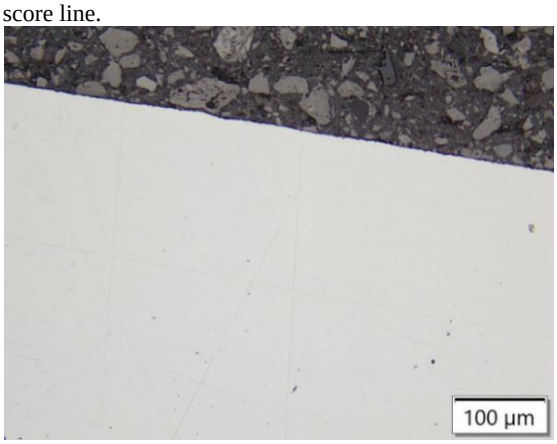

(b) No cracks at the non-corroded area.

Figure 7: Cross-sectional micrograph of the cracks near pits (a) and a non-corroded area with no cracks (b).

The micro-specimen was then electrolytic etched in 10 vol. % oxalic acid to reveal the microstructure. Figure 8 shows a mix mode of trans-granular and intergranular cracking. The general microstructure comprised of austenitic structure, which was typical of 316 stainless steel. Some delta-ferrite stringers were also present, which is commonly found in austenitic stainless-steel sheet material (ASM International, 2004). Note, Figure 8 (b) shows no strong interaction between the delta ferrite stringers and the cracking.

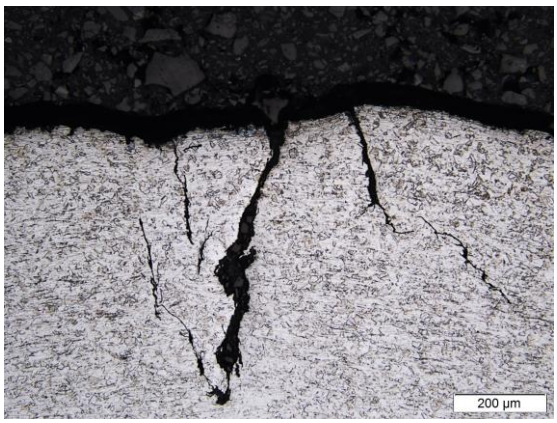

(a) Low magnification image of a crack.

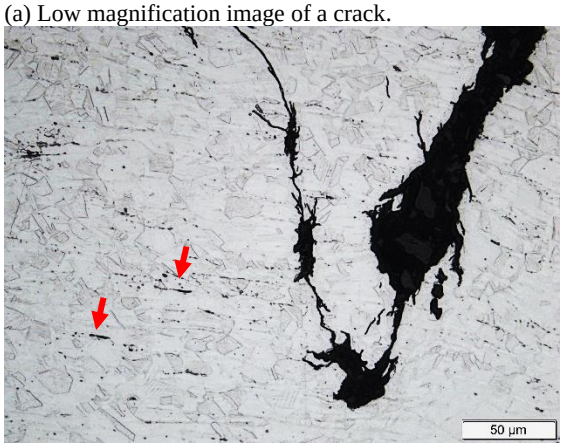

(b) High magnification of image (a), showing austenitic microstructure and several delta ferrite stringers.

Figure 8: A mix of trans-granular and intergranular mode of the cracking. Red arrows represent examples of delta ferrite stringers.

2.3 Hardness Test

Hardness testing was carried out using a Struers Duramin 650 hardness testing machine with a 10-kg load on the micro-specimen described in Section 2.2.2. The hardness results are presented in Vickers hardness (HV10) in Table 2. For comparison, Table 2 also includes the maximum hardness limit of stainless steel 316 grade as per ASTM A240, 2022 and ANSI/NACE MR0175, 2015. The result showed that the average hardness of the disc sample is within the ASTM standard, which indicates that the sample was not work hardened. Also, the hardness was well below the hardness limit for it to be susceptible to sulfide stress cracking. Therefore, the burst disc failure was unlikely caused by sulfide stress cracking/hydrogen embrittlement.

Table 2: Results of hardness tests on the micro-specimen.

	Hardness range (HV10)	**Average (HV10)**
Disc sample	195-206	201
316 stainless steel (ASTM A240, 2022)	< 217	
Limit for sulphide stress cracking (ANSI/NACE MR0175, 2015)	< 248*	

* *Converted from 22 HRC* (ASTM E140, 2019).

3. DISCUSSION

The analysis results on the failed rupture disc described in Section 2 strongly suggest the primary damage mechanisms were pitting corrosion and chloride stress corrosion cracking (Cl-SCC). The disc failed along two of the four score marks and originated from the identified area of pitting and cracking. This led to a change in stress distribution on score lines and caused the base band to be separated. This evidence supports the Cl-SCC damage.

- Numerous pits were present near the cracking area, indicating it was corroded.
- Numerous pits were observed near the cracking, area with some cracks seen passing through or originating from these pits. Chloride was present inside the pits analysed. Chlorides are known to promote pitting corrosion and SCC for austenitic stainless steels (Sedriks, 1996).
- Crack branching was observed on all cracks, which is typical of Cl-SCC cracking. The cracks were branching from the corroded surface and from the likely high-stress area near the crossed-score line.
- There was no cracking in the non-corroded areas.
- The material of the disc was 316 stainless-steel. The 316 stainless steel is known to be susceptible to Cl-SCC (Sedriks, 1996; Parrott and Pitts, 2011). Cl-SCC can occur on stainless-steel 316 grade even in 1 ppm chloride when the surface temperature is above 100°C (Sedriks, 1996).
- The disc sample was not hardened, so sulphide stress cracking/hydrogen embrittlement was not considered as the main damage mechanism.

Cl-SCC requires the following conditions to occur at the same time, and all these conditions were met in the current case of the burst disc.

- Material susceptibility
- Chloride contamination and corrosion
- Wetness
- Tensile stress or residual stress
- Temperature (typically between 60°C and 205°C (API 571, 2020))
- Oxygen

Material Susceptibility

The risk of Cl-SCC in austenitic materials has been linked to nickel content. The greater risk is for the low nickel content of type 304 (8-10.5 wt.%) and 316 (10-13 %) stainless steels. As the failed disc was of 316 stainless-steel, it was susceptible to Cl-SCC.

Two studies by Lichti et al., 1995 and Lichti and Ghaziof, 2022 reported the performance of different types of stainless steels and Ni-based alloys in relation to chloride pitting and Cl-SCC. In these studies, U-bend specimens of each alloy were heated to 105°C. Geothermal steam condensate with 10 ppm chloride added was dripped continuously onto the heated specimens. The results showed that Cl-SCC occurred in nine weeks for 316 stainless-steel. In contrast, no Cl-SCC occurred for nickel-based alloys with a higher nickel content ($\geq$ 57 wt.%), such as Inconel 625 or Hastelloy 276. The maximum pit depth on these corrosion resistant alloys was only less than 20 μm after more than one year of exposure testing.

Chloride Concentration and Corrosion

The cracking area was corroded with some pits observed. The chloride may have come from rainwater. Another possible source of chloride was from the geothermal liquid from the steam and brine vents near the steam line. The cover at the top of the pipe may not have been watertight, so it was possible that rain or geothermal liquids from the surrounding steam vents entered the upward-facing pipe above the disc. The rupture disc was installed 12 years ago, and for most of this time, the external surface of the disc would have been too hot to allow wetness. However, over time there would have been several shutdowns when the external surface may have been wet and then dried; therefore, chloride concentration may have been gradually accumulated.

Wetness

The temperature of the surface of the rupture disc was about 190°C. It would be unusual for wetness to be present for extended periods at this temperature and atmospheric pressure because any water that would drip onto the surface would have been boiled away. However, wetness may have been present during the shutdown-start up period when the disc temperature decreased and then later increased. During shutdown-start up, there would be a temperature cycle between cold (ambient) to hot (190°C). The Cl-SCC may have been occurred during this cycle when wetness and chloride were present.

Tensile Stress or Residual Stress

The stress was likely from the pressure inside the steam pipeline. The highest stress area was likely near the centre of the crossed-score line. The stress experienced by the disc increased as the wall thickness decreased by corrosion and pitting. The residual stress along the crossed-score line may also have contributed to the cracking, for example Figure 2 and Figure 3 show cracks along the cross-section of the score line.

Temperature

From API 571, 2020, the typical temperature range of most concern for external Cl-SCC is 60°C to 205°C, although a laboratory scale study by Prosek, Iversen and Taxén, 2008 has shown that Cl-SCC can occur at 30°C in 20 wt.% of chloride. The Cl-SCC cracking may propagate during the temperature cycle in shutdown-start up periods.

Oxygen

The external surface of the disc convex side is exposed to air atmosphere.

4. CONCLUSION

The burst disc was likely caused by Cl-SCC that led to a stress distribution on venting that was not expected for the petal fashion of failure and caused the base band to be separated. Although stainless steel 316 grade is susceptible to Cl-SCC, a scheduled periodic replacement of the current 316 stainless steel rupture discs is not recommended. SCC failure is not time dependent, and it is not possible to predict the time required for crack initiation. The crack growth rate can vary more than a factor of 50 depending on the environmental conditions according to a report by Parrott and Pitts, 2011.

Therefore, it is difficult to determine the remaining life of the discs from a periodic inspection.

Inconel 625 and Hastelloy 276 are resistant to Cl-SCC, and are, therefore, the recommended material for the rupture disc in a high Cl-SCC risk environment. Inconel 625 may eventually pit but it will likely be very shallow as the disc is not continuously exposed to wetness. Alternatively, a system that can avoid chloride contamination could be designed to prevent ingress of chloride from rain droplets or adjacent steam and brine vent, such as a more reliable covered roof.

5. ACKNOWLEDGEMENTS

The authors express their gratitude to Quest Integrity NZL Limited and Mercury NZ Limited for permission to publish this work.

6. REFERENCES

American Petroleum Institute: API RP 571 Damage Mechanisms Affecting Fixed Equipment in the Refining Industry. (2020).

ANSI/NACE MR0175: Petroleum, petrochemical and natural gas industries — Materials for use in H_2S-containing environments in oil and gas production. (2015).

ASTM A240: Standard Specification for Chromium and Chromium-Nickel Stainless Steel Plate , Sheet , and Strip for Pressure Vessels and for General Applications. (2022).

ASTM E140: Standard Hardness Conversion Tables for Metals Relationship Among Brinell Hardness, Vickers Hardness, Rockwell Hardness, Superficial Hardness, Knoop Hardness, Scleroscope Hardness, and Leeb Hardness. (2019).

ASM International, *ASM Metal Handbook - Metallography and Microstrucutres*. (2004)

Lichti, K. et al.: Corrosion of iron-nickel base and titanium alloys in aerated geothermal fluids. *Proc. World Geothermal Congress*, 4, pp. 2375–2380. (1995).

Lichti, K. and Ghaziof, S.: On the Performance of UNS S32100 vs N08825 Expansion Compensator Materials in Geothermal Applications, *AMPP Annual Conference and Expo*. Texas. (2022)

Parrott, R. and Pitts, H.: *Chloride stress corrosion cracking in austenitic stainless steel*. Health and Safety Executive, UK. (2011).

Prosek, T., Iversen, A. and Taxén, C.: Low temperature stress corrosion cracking of stainless steels in the atmosphere in presence of chloride deposits', *NACE - International Corrosion Conference Series*, 65(2), pp. 105–117. (2008).

Sedriks, A.J.: *Corrosion of Stainless Steels*. 2nd edition. New York: John Wiley & Sons, Inc. (1996).